nature communications

Article

https://doi.org/10.1038/s41467-024-51620-2

Ultrasound-mediated spatial and temporal control of engineered cells in vivo

Received: 3 January 2024

Accepted: 13 August 2024

Published online: 27 August 2024

Check for updates

Filip Ivanovski[1,2,6], Maja Meško[1,6], Tina Lebar[1], Marko Rupnik[1], Duško Lainšček[1], Miha Gradišek[3], Roman Jerala[1,4] & Mojca Benčina[1,4,5]

Remote regulation of cells in deep tissue remains a significant challenge. Low-intensity pulsed ultrasound offers promise for in vivo therapies due to its non-invasive nature and precise control. This study uses pulsed ultrasound to control calcium influx in mammalian cells and engineers a therapeutic cellular device responsive to acoustic stimulation in deep tissue without over-expressing calcium channels or gas vesicles. Pulsed ultrasound parameters are established to induce calcium influx in HEK293 cells. Additionally, cells are engineered to express a designed calcium-responsive transcription factor controlling the expression of a selected therapeutic gene, constituting a therapeutic cellular device. The engineered sonogenetic system's functionality is demonstrated in vivo in mice, where an implanted anti-inflammatory cytokine-producing cellular device effectively alleviates acute colitis, as shown by improved colonic morphology and histopathology. This approach provides a powerful tool for precise, localized control of engineered cells in deep tissue, showcasing its potential for targeted therapeutic delivery.

Controlling cellular activities within deep tissues remains a significant challenge in biomedicine, particularly concerning spatial and temporal manipulation. Optogenetic methods enable the wireless manipulation of engineered cells through the use of genetically encoded light-sensitive proteins and ion channels, allowing the activation or inactivation of cellular processes through ion flux or protein domain interactions[1–6]. However, the limited tissue penetration of light hinders its non-invasive translation to higher organisms.

In contrast, ultrasound offers a solution to the limited tissue penetration of light, presenting a significant advantage for achieving control over cellular processes within deep tissue[7]. Ultrasound with a frequency range of 1–15 MHz has been safely used for medical imaging for decades without adverse effects[8–10]. Furthermore, ultrasound can be focused on an area smaller than 1 mm[2,11], with recent advances in focused ultrasound decreasing this limit to a space as small as 100 × 100 × 300 µm[12]. Low-frequency ultrasound, in particular has better tissue penetration compared to high-frequency ultrasound. Ultrasound has been used to stimulate neurons in various model organisms, from salamanders to mice and non-human primates, both ex vivo and in vivo[7,8,13–17]. Low-intensity ultrasound primarily exerts mechanical effects that can be used to modulate neurons by altering membrane elastic properties[18,19] or by activating mechanosensitive transmembrane proteins[20–23]. Previous studies have shown that ultrasound-induced mechanical perturbations can activate mechanosensitive ion channels, resulting in an influx of Ca^{2+} in a range of transducer frequencies from 0.5 MHz to 30 MHz[20–23]. These frequencies provide both adequate resolution and good penetration of soft tissue, so they are commonly used in diagnostics[10]. Gas vesicles and protein-based microbubbles have also been used as amplifiers for ultrasound-mediated neuromodulation[16,24,25].

Advancements in cancer immunotherapy have significantly increased treatment options. One such option is the use of genetically engineered bacteria that can infiltrate the tumor microenvironment and release therapeutic payloads upon precise stimulation using

[1]Department of Synthetic Biology and Immunology, National Institute of Chemistry, Hajdrihova 19, Ljubljana, Slovenia. [2]Interfaculty Doctoral Study of Biomedicine, University of Ljubljana, Vrazov trg 2, Ljubljana, Slovenia. [3]Faculty of Electrical Engineering, University of Ljubljana, Tržaška c. 25, Ljubljana, Slovenia. [4]CTGCT, Centre of Technology of Gene and Cell Therapy, Hajdrihova 19, Ljubljana, Slovenia. [5]University of Ljubljana, Kongresni trg 12, 1000 Ljubljana, Slovenia. [6]These authors contributed equally: Filip Ivanovski, Maja Meško. e-mail: roman.jerala@ki.si; mojca.bencina@ki.si

focused ultrasound[26,27]. Another option is the use of heat generated by focused ultrasound to enhance the activation of engineered T-cells, thereby promoting the recognition and elimination of target tumor cells[25,28–30]. Although thermal tissue damage shows potential in tumor therapy, it is important to consider its broader implications and potential harm to therapeutic cells[31–33].

Considering ultrasound's impact on mechanosensitive ion channels[20–23], which prompt free calcium ions (Ca^{2+}) influx and activate Ca^{2+}-calmodulin signaling pathways, utilizing a Ca^{2+}-responsive pathway offers an alternative approach to address this challenge.

This study explores the potential of ultrasound as a non-invasive tool for conditionally regulating engineered cellular therapeutic devices in vivo. The study thoroughly investigates the effects of pulsed ultrasound parameters on intracellular Ca^{2+} oscillation in HEK293 cells with the aim of engaging Ca^{2+} signaling rather than the heat shock response. Previous studies have demonstrated that pulsed ultrasound stimulation with low acoustic intensity causes minimal temperature elevation in tissue[34]. However, it induces mechanical perturbations that increase cytosolic Ca^{2+} levels and activate Ca^{2+}-calmodulin signaling pathways[23,35]. This phenomenon has been utilized to regulate gene expression by introducing a synthetic Ca^{2+}-sensitive pathway within cells[36]. Low-intensity pulsed ultrasound is used to induce Ca^{2+} influx and activate a synthetic circuit in implanted engineered cells in mice. This leads to the conditional expression of an anti-inflammatory cytokine, human interleukin-10 (hIL-10). In a murine colitis model, the ultrasound-responsive therapeutic cellular device demonstrates the ability to ameliorate acute colitis, improving colonic morphology and histopathology. The study shows the potential of sonogenetics[17], which combines ultrasound with synthetic biology as a non-invasive therapeutic strategy. Ultrasound's deep tissue penetration enables precise cell stimulation, which holds significant promise for the targeted delivery of anti-inflammatory therapeutics.

Results

Ultrasound triggers calcium influx

In addition to its established role in imaging, ultrasound is capable of activating Ca^{2+}-selective mechanosensitive ion channels at transducer frequencies from 0.5 MHz to 30 MHz. We wanted to find out whether pulsed low-frequency ultrasound can trigger Ca^{2+} influx in HEK293 cells. For cell sonication, we used a custom-built MODUSON-2 ultrasonic wave generator coupled to an amplifier to which an unfocussed 0.5 MHz transducer was connected (Fig. 1A). The acoustic pressure produced by the transducer was indirectly measured using a needle hydrophone in a water tank, evaluating frequencies ranging from 0.2 to 0.5 MHz (Supplementary Fig. 1A). After identifying 0.31 MHz as the frequency (f_0) generating the highest acoustic pressure (Supplementary Fig. 1B), we selected it for further experiments. The measured pressure at distances ranging from 1 to 25 mm from the transducer's face fell between 0.28 to 0.5 MPa (Supplementary Fig. 1C). To eliminate heat-mediated effects during longer insonation periods, we monitored the temperature of the culture media due to the heating of the transducer and introduced active cooling to maintain the culture media temperature constant at 37 °C (Supplementary Fig. 1D).

We performed real-time fluorescence imaging to observe intracellular Ca^{2+} fluctuation during ultrasound stimulation, demonstrating that ultrasound pulses induce Ca^{2+} entry into the cells. Cells were treated with ratiometric Ca^{2+}-sensitive fluorescent dyes, and the changes in the fluorescence intensity served as a reflection of intracellular Ca^{2+} concentration changes (Supplementary Fig. 1E, F). To enable Ca^{2+} influx imaging the ultrasound transducer was positioned in a top-down orientation and immersed in the media (Fig. 1B). In addition to f_0, three other ultrasound stimulation parameters were analyzed: stimulation time (ST) which refers to the duration of one insonation, pulse repetition frequency (PRF) and duty cycle (DC) to assess their impact on Ca^{2+} influx (Fig. 1C). While both 5 and 10 s ST led to strong cellular responses in terms of Ca^{2+} influx, the cells exhibited a faster response to the 10 s pulse compared to the 5 s ST (Fig. 1D). The reduction in Ca^{2+} peak amplitude correlates with shorter ST, as observed previously in neuronal and nucleus pulposus cells[23,35]. Next, we tested PRF with 1 or 4 kHz, along with 8, 16, and 32% DC (Fig. 1E and Supplementary Fig. 1G). Rapid Ca^{2+} influx was achieved with 100 cycles (32% DC) and 1 kHz PRF (Supplementary Fig. 1H). A combination of 25 cycles with 4 kHz PRF (32% DC) triggered a strong Ca^{2+} influx, although the cells exhibited reduced responsiveness to repeated ultrasound stimulation in this case (Supplementary Fig. 1G). Both 1 kHz and 4 kHz PRF induced significant changes in intracellular Ca^{2+} levels. However, the use of 4 kHz PRF required a longer rest interval between stimulations to elicit a repetitive cellular response. Specifically, a 2-minute rest period between ultrasound stimulations was required to return Ca^{2+} levels to their baseline. The addition of gadolinium(III) chloride ($GdCl_3$), a broad-spectrum inhibitor of Ca^{2+} ion channels, effectively inhibited Ca^{2+} influx into the cytosol. This confirms that insonation triggers the influx, which is mediated by Ca^{2+} channels (Fig. 1F). To describe the role of ion channels in ultrasound modulation, we used selective pharmacological blockers for different mechanosensitive channels[23,37] (Supplementary Fig. 2A–E). The peptide inhibitor GsMTx4 targets Piezo1 channels[38]; ruthenium red (RR) targets TRP channels[39]; Pico145 inhibits TRPC1/4/5 channels[40], TTA-P2 targets voltage-gated T-type calcium channels[41] and suramin impedes GPCR signaling by preventing the release of GDP from the G alpha subunit[42]. Of these inhibitors, only GsMTx4 showed a modest but significant reduction in the response of HEK293 cells to ultrasound (Supplementary Fig. 2E), suggesting the involvement of Piezo1 channels in response to ultrasound stimulation. While repeated ultrasound stimulation triggered consecutive Ca^{2+} influx, the cell response became less synchronized after five repetitions, with the amplitude decreasing by approximately 30% (Fig. 1G). In summary, the 0.31 MHz low-intensity pulsed ultrasound with 10 s ST, 1 kHz PRF, and 32% DC induces prominent alternation in Ca^{2+} levels.

Ultrasound activates gene expression via a synthetic calcium-responsive circuit in engineered cells

Given the robust increase in cytosolic Ca^{2+} achieved during insonation, we reasoned that ultrasound could serve as an activator for remotely controlling gene expression in live cells. The nuclear factor of activated T-cells (NFAT) is a transcription factor that plays a pivotal role in translating increased cytosolic Ca^{2+} levels into cellular functions[2]. NFAT activity is regulated through dephosphorylation by the Ca^{2+}-mediated phosphatase calcineurin leading to its translocation to the nucleus. Analogous to the previously published approach in optogenetics[1,2], we adopted the Ca^{2+}-calmodulin-calcineurin-NFAT signaling pathway[43] as a mediator of the ultrasound signal, coupling Ca^{2+} influx with gene transcription (Fig. 2A). To monitor transcriptional activation efficiency, we used a firefly luciferase reporter plasmid containing three NFAT binding sites upstream of a minimal promoter ($_{3NFAT}$_P_{min}-fLuc) (Supplementary Fig. 3A). First, the responsiveness to Ca^{2+} was confirmed using the A21387 Ca^{2+} ionophore, an ion carrier used to increase intracellular Ca^{2+} concentration (hereafter referred to as "ionophore"), in HEK293T cells overexpressing a Myc-tagged human NFAT-c1 isoform ($hNFAT^{FL}$) along with a firefly luciferase reporter plasmid (Supplementary Fig. 3B). Nuclear translocation upon ionophore stimulation was confirmed in real-time using a BFP-tagged $hNFAT^{FL}$ construct by confocal microscopy (Supplementary Fig. 3C). Next, ultrasound stimulation was utilized to activate Ca^{2+}-dependent signaling pathway resulting in NFAT activation. To maintain the sterility, transfected HEK293 cells were insonated using a transducer placed at the bottom of the cell culture plate (Fig. 2B). The parameters used for the ultrasound were previously determined to yield the most consistent Ca^{2+} influx.

https://doi.org/10.1038/s41467-024-51620-2

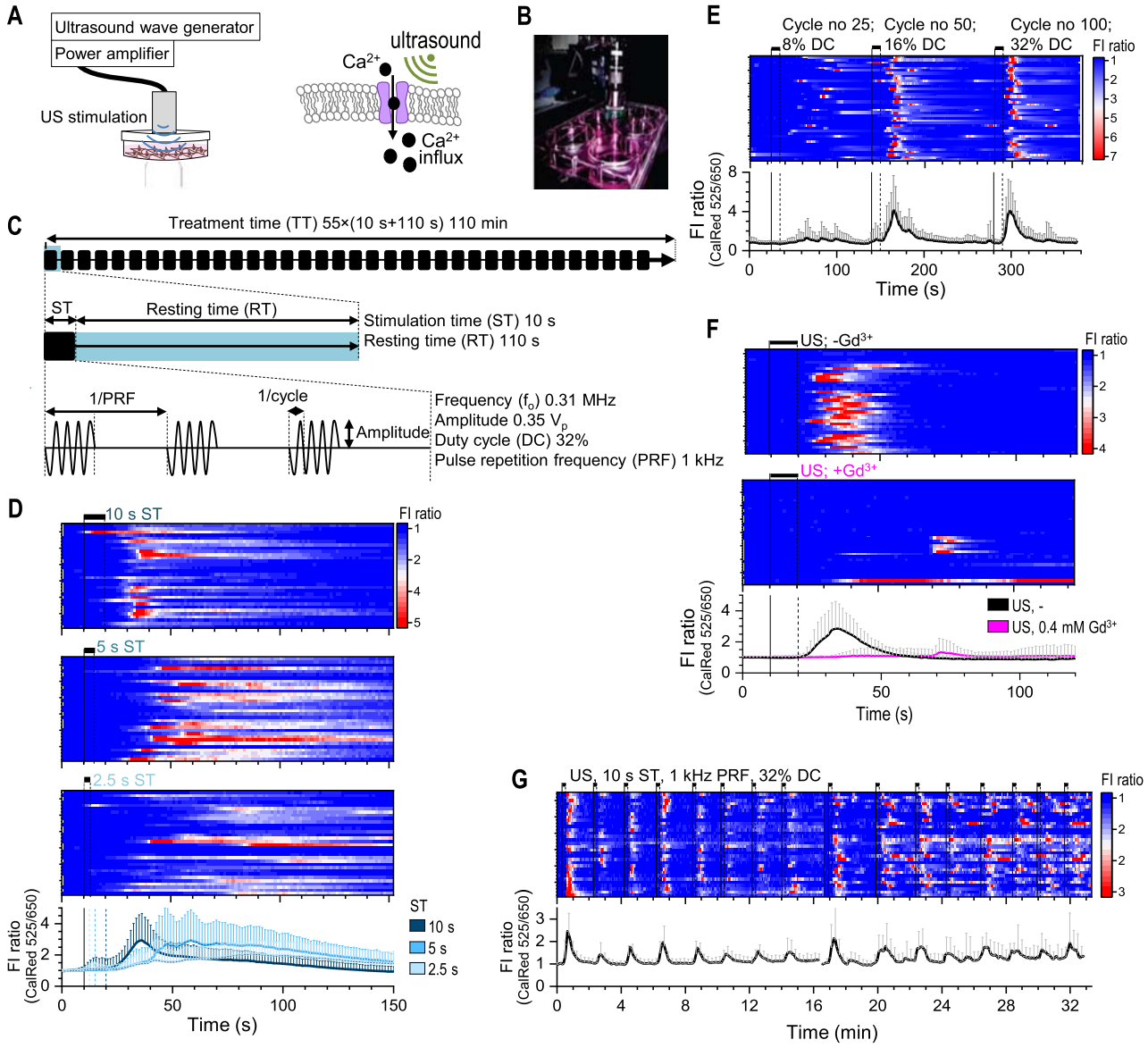

Fig. 1 | Ultrasound as a remote trigger of calcium influx in HEK293 cells. A A diagram illustrating the experimental setup: The ultrasound wave generator (MODUSON-2), connected to a power amplifier, is linked to an unfocused transducer (Olympus V318-SU), which was used for the stimulation of cultured cells. **B** The real-time imaging setup for monitoring Ca^{2+} influx during insonation. The ultrasound transducer was placed top-down in a well, submerged in a medium. The transducer's position was secured with a 3D printed holder that fits into a 6-well plate or a 3.5- cm petri dish. **C** Ultrasound stimulation conditions with adjustable parameters controlled by wave generator: frequency, duration of the stimulation burst - stimulation time (ST) and resting time, pulse repetition frequency (PRF), duty cycle (DC), and amplitude are depicted. **D**–**G** The response of HEK293 cells to insonation. Various conditions of ultrasound pulse were tested on HEK293 cells stained with the Ca^{2+}-sensitive dye. **D** Different ST (2.5, 5, and 10 s) with fixed 1 kHz PRF and 32% DC ($n = 32$ individual cells for each group), and (**E**) different DC (8, 16, and 32 %) with fixed ST (10 s) and PRF (1 kHz) were tested. $n = 40$ individual cells. **F** $GdCl_3$ (0.4 mM) inhibited the Ca^{2+} influx triggered by ultrasound (10 s ST, 1 kHz PRF, 32% DC). $n = 36$ individual cells for Gd^{3+} - and 40 for Gd^{3+}+ group. **G** The Ca^{2+} oscillations are triggered by a consecutive repeated sequence of 10 s ST followed by a 110 s resting period. Changes in fluorescence intensity (FI) ratio (indicative of Ca^{2+} activity) during insonation are presented as a heatmap. Each row presents the Ca^{2+} activity of an individual cell ($n = 34$ individual cells). The FI ratio of CalRed at 488 nm-excitation over time was calculated for individual cells normalized to the pre-stimulated average FI ratio. The average FI ratios (with standard deviation) were calculated and are presented below the heatmap with black vertical lines indicating the periods of ultrasound stimulation. Source data are provided as a Source Data file. Items in (**A**) are adapted from ref. 36 released under Creative Commons Attribution 4.0 International (CC BY 4.0).

Ultrasound did not activate the native NFAT signaling pathway in HEK293 cells, as shown by unchanged luminescence in cells transfected with $_{3NFAT}$_P_{min}-fLuc (Fig. 2C, second bar). Similarly, in wild-type Jurkat cells, the expression level of IL-2 and TNF-α – genes regulated by NFAT transcription factors – remained unchanged in stimulated cells compared to non-stimulated cells (Supplementary Fig. 3D, E). In addition, other downstream calcium-responsive signaling pathways, including p38 kinase signaling[44] and NF-κB[45] or CREB transcription factor signaling[46] were not activated by ultrasound stimulation (Supplementary Fig. 3F–H).

As anticipated, acoustic stimulation led to the translocation of overexpressed BFP-tagged NFAT from the cytosol to the nucleus (Fig. 2D). The ultrasound-induced expression of the firefly luciferase reporter was detected in HEK293 cells overexpressing $hNFAT^{FL}$. Furthermore, the activation of reporter expression via the calcineurin/NFAT pathway was confirmed by incubating cells with an inhibitor of

https://doi.org/10.1038/s41467-024-51620-2

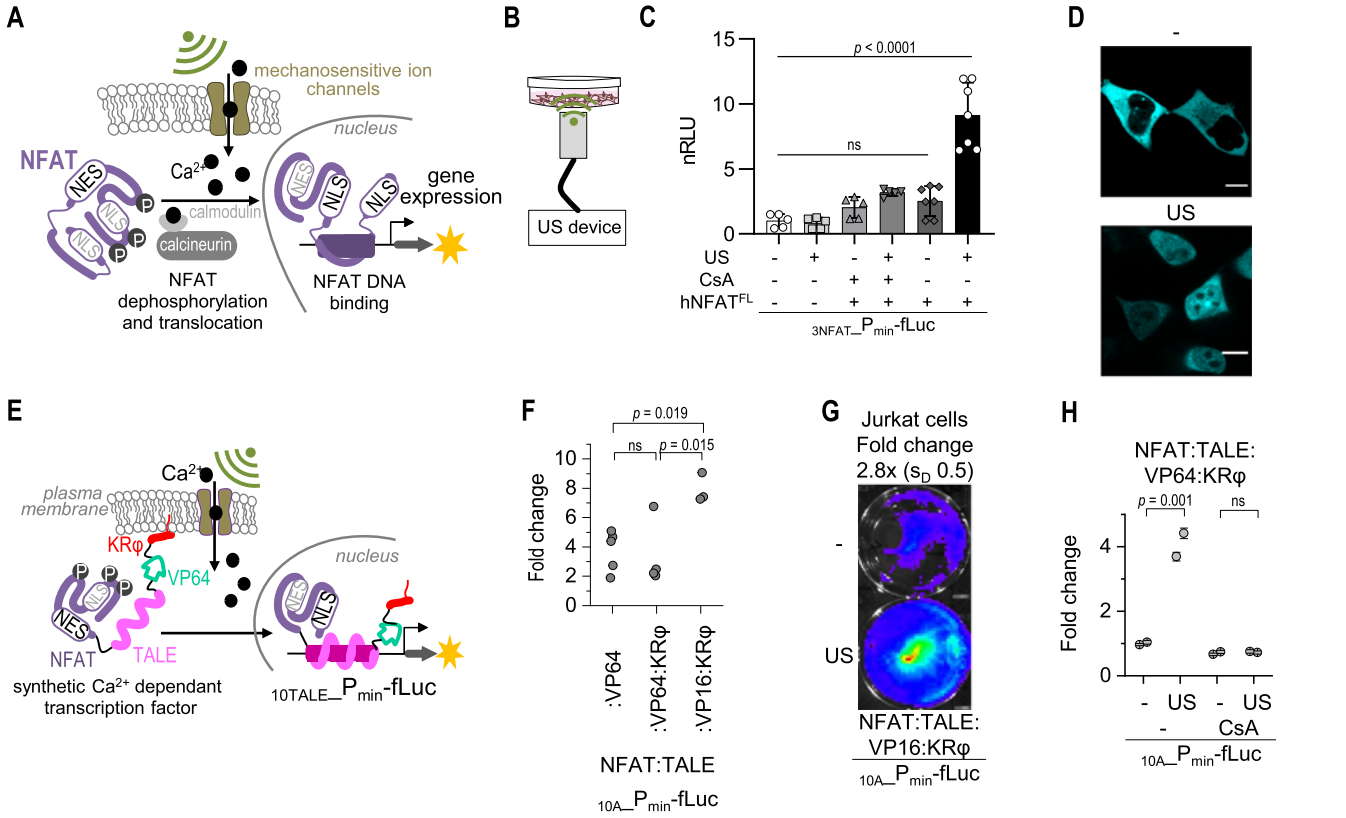

Fig. 2 | Ultrasound-mediated activation of the engineered calcium-responsive transcription factor. A Scheme of the Ca^{2+}-calmodulin-NFAT signaling pathway activated by ultrasound. Insonation triggers a Ca^{2+} influx that activates the calmodulin-calcineurin-NFAT pathway, leading to NFAT-regulated gene expression. **B** Experimental setup for ultrasound stimulation of cultured cells. **C** Transcriptional activity of NFAT in insonated HEK293 cells, with or without overexpressed $hNFAT^{FL}$ and CsA treatment. HEK293 cells transfected with $hNFAT^{FL}$, reporter plasmid $_{3NFAT}P_{min}$-fLuc, and phRL-TK (rLuc) were stimulated with ultrasound. Firefly luciferase activity was measured 4 h later. CsA (1 μM) was added 30 minutes before insonation. Bars represent the mean ± SD; $n = 5, 5, 5, 5, 7$ and 7 biological replicates left to right. **D** Confocal microscopy images of HEK293 cells transfected with $hNFAT^{FL}$:BFP encoding plasmid (100 ng). Scale bar, 10 μm. Images are representative of three independent experiments. **E** Scheme of ultrasound-triggered Ca^{2+}-dependent activation and translocation of the engineered NFAT-based transcription factor. Insonation activates reporter gene transcription in (**F**) HEK293 cells and (**G**) Jurkat cells. **F** HEK293 cells were transfected with the CaTF, reporter plasmids $_{10A}P_{min}$-fLuc, and phRL-TK (rLuc). Reporter activity was measured 3-4 h after insonation. $n = 5, 4$, and 3 biological replicates left to right. **G** Jurkat cells were transiently transfected with NFAT:TALE:VP16:KRφ and reporter plasmid $_{10A}P_{min}$-$fLuc^{PEST}$, divided, and one well was insonated. Firefly luciferase activity was measured 3-4 h post-ultrasound stimulation. Images are representative of 2 independent experiments. **H** Transcriptional activity of engineered CaTF post-ultrasound and +/− CsA treatment. HEK293 cells were stimulated with ultrasound one day after transfection, with or without CsA (1 μM) added 30 min before treatment. Reporter activity was measured 3-4 h post-treatment. Dots represent the mean ± SD; $n = 2$ biological replicates. **C**, **F**, **H** *P*-values were calculated with one-way ANOVA with Tukey's post test. Amounts of transfected plasmids used in experiments (**C**, **F**, **H**) and (**G**) are listed in Supplementary Tables 3 and 4, respectively. Statistics are depicted in Supplementary Data 1. Source data are provided as a Source Data file. Items in (**A**, **E**) adapted from ref. 36 released under Creative Commons Attribution 4.0 International (CC BY 4.0).

calcineurin, cyclosporine A (CsA) (Fig. 2C). Ultrasound stimulation at the specified parameters did not cause any significant decrease in cell viability (Supplementary Fig. 3I) and metabolic activity (Supplementary Fig. 3J) measured 24-h post-insonation, compared to non-insonated cells.

When engineering synthetic biological circuits, it is essential to ensure that their functionality is independent of the host cell's endogenous processes, thus avoiding unintended regulation of autologous genes. For this purpose, we employed and improved previously characterized engineered Ca^{2+}-responsive transcription factors (CaTFs), based on murine NFAT and a designed transcriptional-activator-like effector (TALE) DNA-binding domain[36]. Furthermore, the KRφ peptide-tagged membrane-bound CaTFs are released into the cytosol and translocated into the nucleus following Ca^{2+} influx. Our premise was that ultrasound should regulate the activation of these CaTFs without simultaneously activating the endogenous NFAT-responsive genes. In addition to the previously characterized murine CaTFs[36], we designed two additional CaTFs by substituting the VP64 activation domain with the less potent VP16 domain (Supplementary Fig. 4A, B) to reduce activation in unstimulated cells (Supplementary Fig. 4E, F). The engineered CaTFs (NFAT:TALE:VP16 or NFAT:TALE:VP16: KRφ) translocated to the nuclei following Ca^{2+} influx (Supplementary Fig. 4C, D) and mediated robust ionophore-triggered transcription from the synthetic promoter with 10 repeats of the TALE binding site upstream of a minimal promoter ($_{10TALE}P_{min}$-fLuc) (Supplementary Fig. 4C, D). As expected, the CaTF anchored to the plasma membrane using the KRφ peptide, which partitions preferentially to anionic lipids in an ionic strength-dependent manner[47], exhibited a higher signal-to-background ratio due to reduced activity in non-stimulated cells (Supplementary Fig. 4C–F).

The dissociation of KRφ peptide from the plasma membrane is a result of calcium influx, which shields the membrane charge, activates phospholipase C for PIP_2 hydrolysis and activates the lipid scramblase, which translocates phosphatidylserine to the outer leaflet. Ionophores, sonication, antimycin, and dibucaine can trigger this release[47–49]. $GdCl_3$, a non-specific inhibitor of plasma membrane cation channels, blocked the release of the KRφ peptide from the membrane even in the presence of thapsigargin (TG), which releases calcium from the

endoplasmic reticulum, suggesting that plasma membrane mechanosensitive channels have a greater impact on the release of the synthetic construct (Supplementary Fig. 5A). Furthermore, the release of the KRφ peptide is independent of NFAT (Supplementary Fig. 5B) and increasing concentrations of KRφ peptide do not disrupt calcium influx within the cell (Supplementary Fig. 5C).

Subsequently, we investigated the ultrasound as a remote trigger of transcriptional activation (Fig. 2E, F). HEK293 cells expressing the engineered transcription factor and reporter under the control of the TALE promoter were insonated using a transducer operating at 0.31 MHz and placed beneath the petri dish (Fig. 2B). Ultrasound-induced transcriptional activity was shown to depend on PRF (Supplementary Fig. 6A), stimulation time (Supplementary Fig. 6B), the amount of transcription factor (Supplementary Fig. 6C), and the duration of treatment time (Supplementary Fig. 6D). The combination of pulse parameters with an operating frequency 0.31 MHz, a ST 10 s and a PRF 1 kHz with a total treatment duration of two hours, was most effective in inducing reporter expression. We observed translocation of NFAT:TALE:VP16:KRφ into the nucleus after ultrasound stimulation (Supplementary Fig. 6E) and a 2- to 10-fold transcriptional activation in HEK293 cells transfected with NFAT:TALE:VP16:KRφ, NFAT:TALE:VP64:KRφ and NFAT:TALE:VP64 (Fig. 2F). In addition, ultrasound treatment activated the expression of firefly luciferase in Jurkat cells, further demonstrating the system's versatility across different cell lines (Fig. 2G). Pretreatment of cells with CsA (Supplementary Fig. 6F) attenuated transcriptional activity, confirming the involvement of the calcineurin-NFAT signaling pathway in ultrasound-stimulated regulation of gene expression (Fig. 2H and Supplementary Fig. 6G). Furthermore, the addition of $GdCl_3$ to cells transfected with the engineered CaTF and reporter plasmid and stimulated with ultrasound showed no difference between stimulated and non-stimulated cells, as expected due to the inhibition of mechanosensitive channels (Supplementary Fig. 6H). As expected, acoustic stimulation did not result in the translocation of overexpressed KRφ-labeled NFAT:BFP from the cytosol to the nucleus when cells were pretreated with $GdCl_3$ (Supplementary Fig. 6I, J).

Ultrasound as a remote trigger for a spatially confined in vivo stimulation of the engineered cells

To mitigate the side effects of systemic therapy, a localized application of therapeutics is preferable. Similar to optogenetic[1–5], low-intensity pulsed ultrasound could be used for spatially controlled expression of target therapeutic genes[25,28–30]. We tested whether insonation can activate subcutaneously implanted cells in a mouse without adding acoustic actuators such as gas vesicles (Fig. 3A). HEK293T cells transiently transfected with a plasmid encoding CaTF and a firefly luciferase reporter plasmid, were implanted into the hind leg of a mouse and subjected to insonation. To ensure tissue safety during prolonged sonication, we adhered to FDA's established safety guidelines for diagnostic ultrasound ($I_{SPTA} \leq 720$ mW/cm^2, MI ≤ 1.9, or derated $I_{SPPA} \leq 190$ W/cm^2). Our parameters, including an I_{SPPA} of 2.6 W/cm^2, an I_{SPTA} of 830 mW/cm^2 and a MI of 0.5 for a 0.5 MHz transducer, and I_{SPPA} of 14.7 W/cm^2, an I_{SPTA} of 1.47 W/cm^2 and a MI of 0.66 for 1 MHz transducer, were chosen to be well below or around the maximum values prescribed by the regulatory authorities[50,51]. The temperature remained constant at 37 °C during insonation, indicating that there was no overheating at the stimulation site (Supplementary Fig. 7A), and no mechanical changes were observed in the skin and muscle tissue due to the two-hour ultrasound exposure (Supplementary Fig. 8).

Although weak background expression of the reporter was observed in non-insonated cells, insonation resulted in an average 4-fold increase in reporter expression (Fig. 3B, C and Supplementary Fig. 7B). The activation of the cells by ultrasound is spatially limited. This is shown by the fact that only insonated cells implanted in the right hind leg were activated, whereas no activation was observed in the same cell type implanted in the left hind leg (Fig. 3B and Supplementary Fig. 7B).

To test whether the engineered cells can promote local expression of therapeutics, we coupled the ultrasound-activated transcription factor with the expression of a transgenic human anti-inflammatory cytokine, interleukin-10 (IL-10)[52] (Fig. 3A). The tested engineered CaTFs that exhibited low transcriptional activity in uninduced cells were activated following ultrasound stimulation, showing over 4-fold difference between the stimulated and unstimulated states (Fig. 3D, E); with augmented expression of hIL-10 for NFAT:TALE:VP64:KRφ, although to a lower extent than the ionophore induced hIL-10 (Supplementary Fig. 9A).

The study was extended to explore the possibility of using pulsed ultrasound to activate engineered cells in deep tissues, such as the peritoneal cavity (Fig. 3F, G). To account for possible variations in luminescence measurements in vivo due to differences in the depth of cell implantation, we paid particular attention to the injection of artificial cells in ECM gel into the peritoneal cavity. To address this issue, we additionally co-transfected the cells with constitutively expressed near-infrared fluorescent protein (iRFP). In this way, we were able to normalize the luminescence intensity of fLuc with the fluorescence intensity of iRFP in the region of interest and thus assess the efficiency of transfection and local stimulation. The genetically engineered HEK293T cells implanted in the peritoneal cavity of mice responded to ultrasound stimulation, as shown by the activation of the firefly luciferase reporter gene. Although weak background expression of the reporter was observed in non-insonated cells, ultrasound stimulation resulted in an average 3-fold increase in reporter expression, confirming the utility of sonogenetics approaches for the control of target cells in deep tissues.

Subsequently, cells encapsulated in ECM gel expressing CaTF and hIL-10 under the TALE promoter were injected into the peritoneal cavity. Intraperitoneally implanted engineered cells were acoustically stimulated, thereby promoting the expression and secretion of hIL-10 (Fig. 3F, H). Six hours after stimulation, the amount of hIL-10 detected was approximately 1 ng/ml for the genetically engineered cells expressing NFAT:TALE:VP64 (with high hIL-10 background, Supplementary Fig. 9B) and approximately 0.4 ng/ml for NFAT:TALE:VP64:KRφ (Fig. 3H) which is about 100-fold and 40-fold the basal serum concentration in healthy humans, respectively[53]. No inflammatory cytokines were detected in serum after ultrasound treatment; mIL-1β, mIL-6, and mTNF-α (below LLOD) in mice. All in all, engineered cells can be activated by ultrasound stimulation, leading to the production of therapeutics such as hIL-10.

To emphasize the potential of our system for non-invasive, remote control of target cells and to avoid the use of heterologous cells, the plasmids were electroporated directly into the hind legs of mice and stimulated with ultrasound (Fig. 3I). The results were similar to those obtained with implanted cells expressing firefly luciferase (Fig. 3J and Supplementary Fig. 7C) and secreting hIL10 (Fig. 3K), but showed lower overall production of the desired protein, likely due to fewer cells being electroporated. This provides further opportunities to utilize our system for non-invasive remote control of target cells.

Application of the therapeutic cellular device in vivo for the treatment of acute colitis in mouse model

To demonstrate the therapeutic potential of genetically engineered cells and to evaluate the in vivo functionality of a therapeutic cellular device, we used a mouse colitis model induced by a nine-day exposure to 4% DSS (dextran sodium sulfate) in an outbred CD-1 mouse line[54]. Subsequently, an ultrasound-sensitive therapeutic cellular device expressing hIL-10 was implanted into the peritoneal cavity (Fig. 4A, B). The engineered cells were encased in hollow modified polyvinylidene difluoride fibers (mPVDF) with 20 nm pores, which we refer to as a therapeutic cellular device (Fig. 4A). This envelope serves two

https://doi.org/10.1038/s41467-024-51620-2

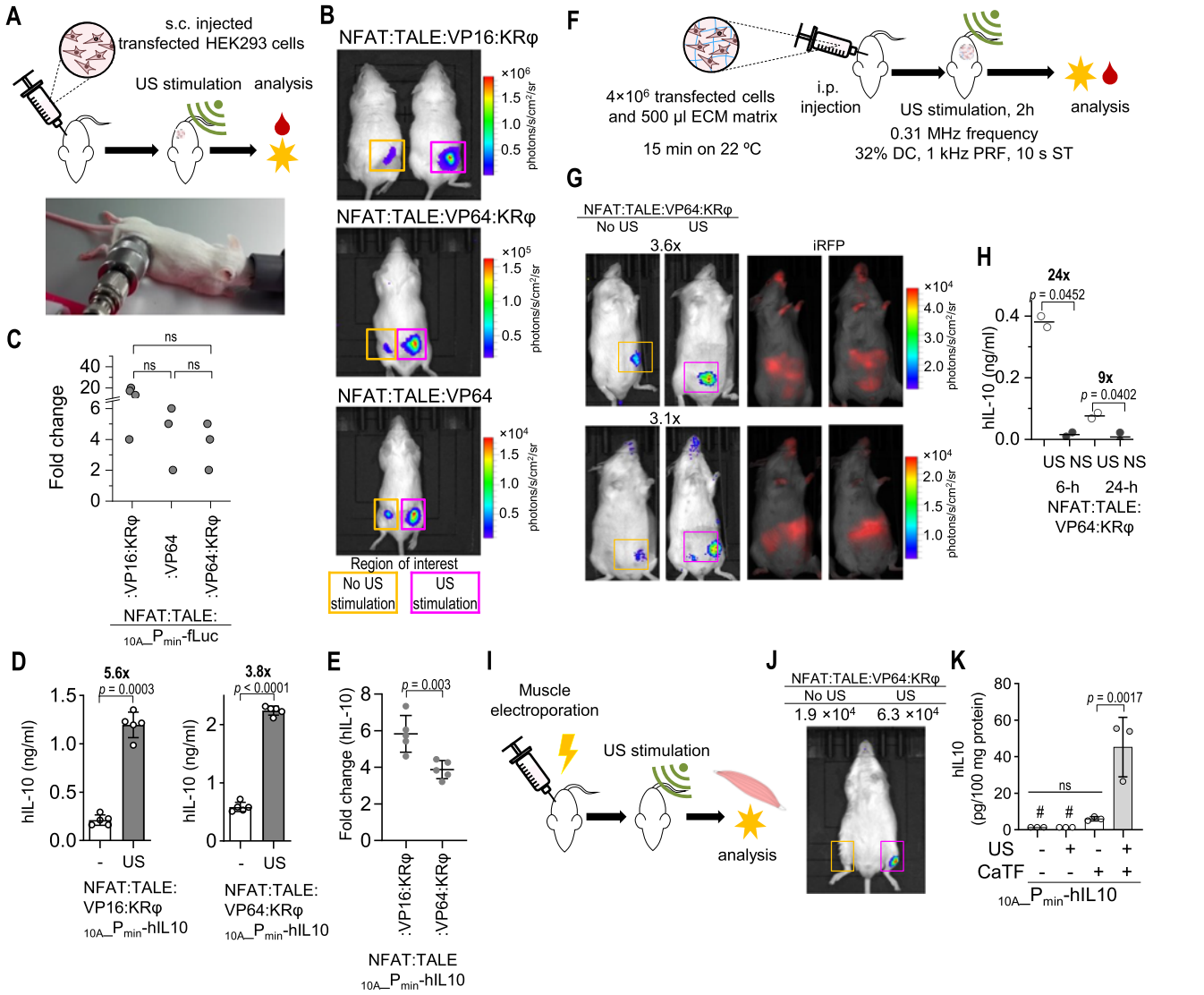

Fig. 3 | Ultrasound-mediated transcriptional activation of implanted engineered cells in vivo. A Experimental setup for ultrasound activation of subcutaneously injected cells with analysis of target gene expression (fLuc or hIL-10) post-ultrasound treatment. **B** HEK293T cells, transfected with CaTF and reporter plasmid $_{10A}$_P$_{min}$-fLuc, were subcutaneously injected and stimulated with ultrasound. Luminescence was imaged four hours later. **C** Fold change between ultrasound-stimulated and unstimulated cells in mice. Results from multiple mouse experiments are combined (see also Supplementary Fig. 7B). $n = 4$, 3, and 3 mice per group left to right. **D**, **E** Serum concentration of transgenic hIL-10 determined 4–6 h post-ultrasound treatment using ELISA. Bars (**D**) and lines (**E**) represent the mean ± SD from five biological replicates. **F** Experimental setup for ultrasound activation and analysis of intraperitoneally injected engineered cells captured in ECM gel. **G** HEK293T cells transfected with NFAT:TALE:VP64:KRφ, reporter plasmid $_{10A}$_P$_{min}$-fLuc, and iRFP as a transfection control were injected intraperitoneally and stimulated with ultrasound. Fluorescence of iRFP and luminescence of fLuc were imaged six hours later. **H** Transcription of hIL-10 activated through insonation of intraperitoneally injected HEK293T cells transfected with NFAT:TALE:VP64:KRφ and reporter plasmid $_{10A}$_P$_{min}$-hIL-10. Blood samples were collected 6 and 24 h post-insonation to determine hIL-10 levels using ELISA. $n = 2$ mice per group. **I** Experimental setup for ultrasound activation of electroporated cells with analysis of target gene expression (fLuc or hIL-10) post-treatment. **J** Transcriptional activity of ultrasound-activated engineered transcription factor in the hind leg muscle of electroporated mice. Mice were electroporated with NFAT:TALE:VP64:KRφ and reporter plasmid $_{10A}$_P$_{min}$-fLuc (see also Supplementary Fig. 7C). **K** Left and right hind leg muscles of mice were electroporated with NFAT:TALE:VP64:KRφ and reporter plasmid $_{10A}$_P$_{min}$-hIL-10 or reporter plasmid alone, and stimulated with ultrasound one day later. Four hours post-stimulation, muscles were collected, and ELISA was used to determine hIL-10 levels. $n = 3$ mice per group. Cytokine levels were normalized by total protein content. Results in groups marked with a hash (#) were below LLOD, so the values were substituted for LLOD (2 pg ml^{-1}) divided by the square root of 2. *P*-values were calculated using one-way ANOVA with Tukey's post-test (**C**, **K**) and paired *T*-test, two-tailed (**D**–**H**). Amounts of transfected plasmids are listed in Supplementary Tables 5 and 6. Statistics are depicted in Supplementary Data 1. Source data are provided as a Source Data file.

important purposes: it protects the genetically modified cells from the host immune system and facilitates the exchange of nutrients and secrete therapeutic proteins, while the genetically modified cells are safely enclosed in the nine-day experimental setting[55]. IL-10, known for its efficacy in reducing inflammation in various colitis models and in human inflammatory bowel disease, was used as a therapeutic output[56–58]. Considering that hIL-10 is effective in mice, we retained hIL-10 as a therapeutic output[59,60], so that it was possible to distinguish between the production of the therapeutic protein and its plasma concentration in mice based on its distinctness from native IL-10.

For the acoustic stimulation of the therapeutic device, we used an unfocussed 1 MHz transducer with a higher maximum sound pressure and a higher cavitation threshold. The normalized maximum sound pressure generated by the transducer was measured with a hydrophone at a 1 MHz frequency on a 2D plane and at different distances from the surface of the transducer (Supplementary Fig. 10A, B). With a

https://doi.org/10.1038/s41467-024-51620-2

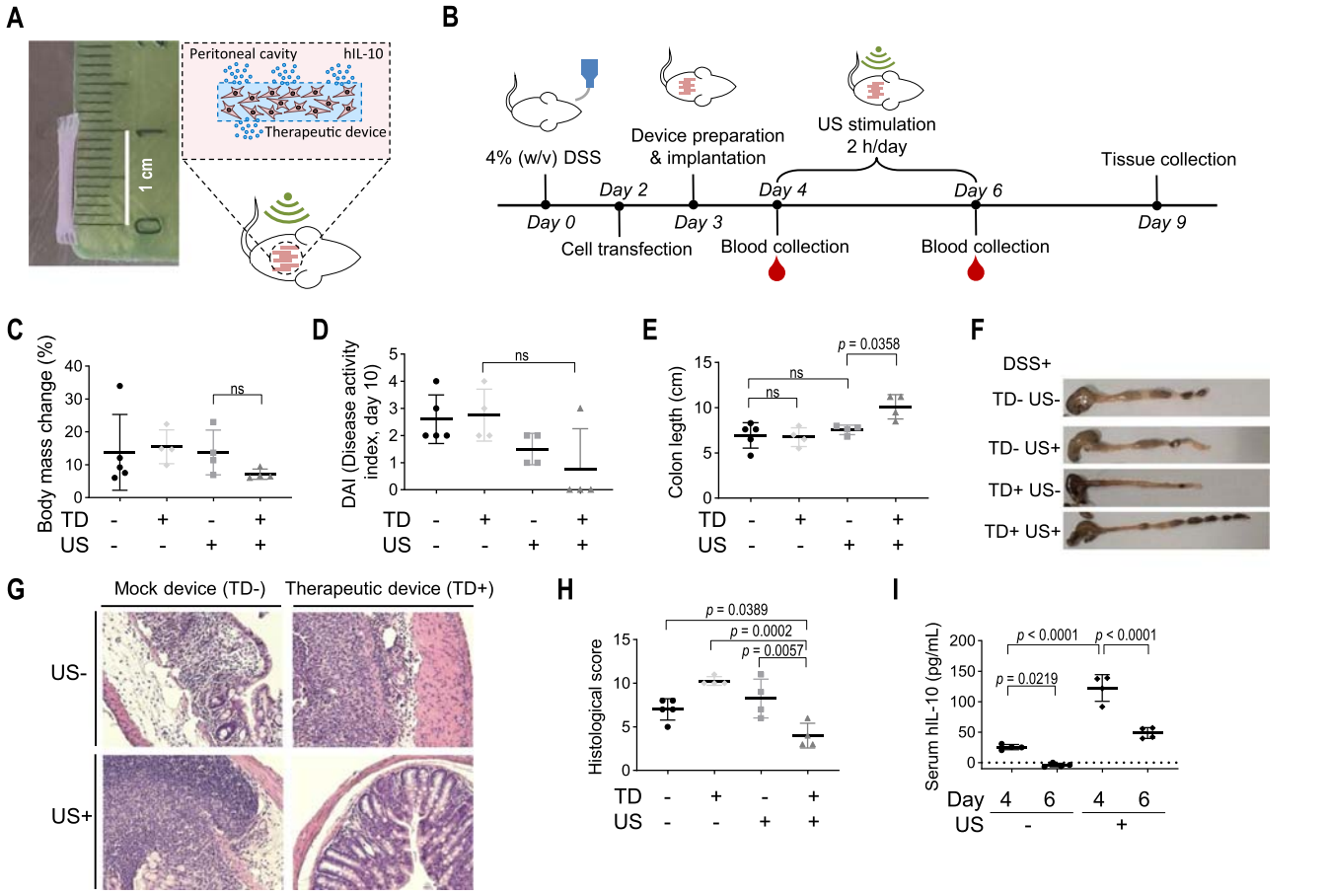

Fig. 4 | The ultrasound-mediated therapeutic cellular device ameliorates acute DSS-induced colitis. A Prepared therapeutic cellular device (left) and experimental setup of i.p. implanted therapeutic cellular device in mouse (right). HEK293T cells were transfected with NFAT:TALE:VP64:KRφ, and reporter plasmid $_{10A}$_P_{min}-hIL-10 enclosed in mPVDF fibers. **B** Mice were administered either 4% DSS drinking water or normal drinking water for 9 days. On day 9, the mice were euthanized and tissue was collected. **C** Weight change of the mice on day 9 compared to day 0. After 9 days of 4% DSS drinking water or normal drinking water administration (**D**) disease activity index was scored before euthanizing mice and harvesting colons. **E** Colon lengths were measured (see also Supplementary Fig. 10E), (**F**) colon morphology and (**G**) histopathology (see also Supplementary Fig. 11) were assessed and (**H**) histological score was calculated. **I** hIL-10 was determined in serum samples collected 6 h after treatment on day 4 and day 6. **C**–**E**, **H**, **I** $n = 5, 4, 4$, and 4 mice per group left to right. The lines represent mean ± SD. *P*-values were calculated with one-way ANOVA with Tukey's post test. Amounts of transfected plasmids are listed in Supplementary Table 5. Statistics are depicted in Supplementary Data 1. TD = therapeutic cellular device. Source data are provided as a Source Data file.

driving voltage of 180 V_{pp} at the transducer, a 10% DC, and a PRF of 1000 Hz, we measured a peak maximum acoustic pressure of 0.66 MPa at the surface of the transducer. Compared to the 0.5 MHz transducer, the higher amplitude of the calcium inflow and the longer duration of the peak were characteristic of the 1 MHz transducer (Supplementary Fig. 9D).

Prior to performing the in vivo experiment, we performed an in vitro evaluation of the therapeutic device (enclosed engineered HEK293T cells). This revealed a significant increase in hIL-10 production in stimulated cells (2.5 ng in total) compared to unstimulated cells on two consecutive days, with samples taken 6 h after a two-hour treatment period (Supplementary Fig. 10C). Furthermore, both the stimulated and unstimulated therapeutic devices maintained approximately 75% cell viability after three days of encapsulation (Supplementary Fig. 10D). The hIL-10 expression was dependent on the presence of CaTF (Supplementary Fig. 9C).

In the following in vivo experiment, we implanted the therapeutic cellular device and a sham device (containing non-transfected HEK293T cells) three days after the start of DSS exposure. The cells were stimulated for 2 h per day for 3 days (Fig. 4B). The groups with the implanted sham device were used to verify that the surgical procedure and ultrasound stimulation did not affect the drinking behavior of the mice so that the amount of DSS consumed remained unaffected. Importantly, a reduction in colon shortening was observed in the ultrasound-treated group with implanted therapeutic cellular device compared to other control groups (Fig. 4E and Supplementary Fig. 10F). The insonated implanted therapeutic cellular device significantly improved intestinal morphology (Fig. 4F and Supplementary Fig. 10E). In addition, it led to a notable reduction in weight loss (Fig. 4C and Supplementary Fig. 10G) and a decrease in the disease activity index as indicated by stool consistency and blood in the stool (Fig. 4D and Supplementary Fig. 10H). In addition, the therapeutic device showed an improvement in colon histopathology (Fig. 4G and Supplementary Fig. 11) and histological score (Fig. 4H and Supplementary Fig. 10I), characterized by reduced infiltration of lymphocytes and neutrophil granulocytes, less damage to the crypt, and the absence of ulcers. As the experiment progressed, we observed lower concentrations of hIL-10 in the serum on the sixth day after stimulation (Fig. 4I). The decrease in hIL-10 concentrations observed over time is to be expected due to the transient nature of the genetically modified cells, which represents a limitation of their long-term therapeutic capacity. This decline is likely due to intracellular plasmid degradation,

spontaneous loss, and dilution during cell division, a well-documented phenomenon in transiently transfected cells[61,62].

In addition, a comparative analysis was performed to evaluate the effects of treatment between the local release of hIL-10 from a therapeutic cellular device activated by low-intensity pulsed ultrasound (Fig. 4) and a systemic treatment approach with a dose of 2.5 ng recombinant human IL-10 (rhIL-10) administered intraperitoneally for three consecutive days as therapy for acute colitis (Supplementary Fig. 10E–I). The dose for systemic administration was objectively determined by the secretion of hIL-10 from the therapeutic device during a single ultrasound activation event (Supplementary Fig. 10C). As predicted, systemic administration of rhIL-10 showed minimal therapeutic efficacy in the treatment of acute colitis, likely due to the administration of a low dose. Optimal therapeutic results in the treatment of acute colitis in humans usually require a minimum dose of 1 μg per kg body weight[63,64], which is about ten times higher than the dose used in our study. The pharmacokinetics of systemically administered rhIL-10 suggest a rapid onset of action with a mean half-life of 2.6 h[64], a factor that most likely contributes to its reduced therapeutic effect compared to the localized sustained release facilitated by therapeutic cellular devices at the site of application. This comparative analysis emphasizes the potential advantages of ultrasound-guided local release strategies and demonstrates their superiority over the limitations observed with systemic administration.

These results emphasize the potential of an ultrasound-responsive switch that enables precise spatial modulation of engineered cells. This technology provides a versatile platform for targeted protein expression and therapeutic intervention. The demonstrated ability to remotely activate and limit cellular activity in deep tissues underlines the promising role of this sonogenetics approach for localized and remote therapy.

Discussion

The results of this study present a sonogenetics approach to control the transcriptional activity of mammalian cells harboring engineered transcription factors using ultrasound, demonstrating its efficacy in mediating Ca^{2+} influx-based regulation of the target genes in vivo. To achieve this, we optimized the insonation parameters that induce robust intracellular Ca^{2+} entry, ensuring sustained cellular activities. We found that a 0.5 MHz transducer operating at a 0.31 MHz center frequency generated sufficient acoustic pressure to elevate intracellular Ca^{2+} levels. While cells demonstrated the ability to respond repetitively to ultrasound pulses, the first Ca^{2+} peak always exhibited the highest amplitude. The reduced amplitude in subsequent pulses may be attributed to factors such as ion channel desensitization[65], depletion of intracellular Ca^{2+} stores, and depolymerization of the target cell's actin cytoskeleton[23]. Our findings, supported by the inhibition of Ca^{2+} influx with chemical blockers and peptide inhibitors, confirm previous claims that ultrasound-induced Ca^{2+} entry indeed relies on the activation of ion channels at the plasma membrane. Notably, it has been previously documented that including but not limited to, the TRPC1, Piezzo1, TRPA1, and ASIC1a are involved in the ultrasound-mediated mechanotransduction with Ca^{2+} entry and depolarization of plasma membrane[17,20–23].

To achieve precise activation of any target gene while preventing unintended activation of endogenous NFAT targets, we used and improved a synthetic NFAT-based transcription factor with the NFAT-DNA binding domain replaced with a customizable, designable DNA-binding domain[36]. This modular approach allows for the substitution of the NFAT-DNA binding domain with diverse DNA-binding domains, not just TALEs, as long as they lack intrinsic nuclear translocation signals. To improve the signal-to-background ratio, a KRφ anchor peptide was tethered to the C-terminus of the transcription factor[47,48]. This resulted in low transcriptional activity in uninduced cells but also led to a reduction in the overall output signal. The decrease in transcriptional activity could be attributed to the incomplete release of the NFAT-KRφ transcription factor from the plasma membrane post-insonation[36].

Recognizing the challenge of translating findings from in vitro cell stimulation in glass-bottom Petri dishes to an in vivo mouse model, we hypothesized that by fine-tuning ultrasonic stimulation parameters in the in vitro setting, we could establish optimal conditions that might be effectively applied in the in vivo context. This hypothesis was substantiated by the results of in vivo experiments including the mouse model of acute colitis, demonstrating the translatability and effectiveness of the optimized parameters in a real-world, in vivo scenario. We demonstrated that ultrasound stimulation led to significant increases in reporter gene expression in both subcutaneously and intraperitoneally implanted cells in mice, suggesting the potential of this approach for non-invasive modulation of cells in deep tissues.

Furthermore, we have linked ultrasound-activated transcription factors with the expression of the anti-inflammatory cytokine, IL-10, demonstrating the potential of ultrasound in promoting local expression of therapeutic. Although the secretion of hIL-10 was well above the basal level in healthy humans[53], a two-hour insonation was required to achieve robust transcriptional activity. According to optogenetic studies[2], an increase in the amplitude and full-width half maximum (FWHM) of Ca^{2+} influx can lead to a higher cumulative load of Ca^{2+}, which shortens the required time for NFAT activation. It is important to note, however, that light-induced transcriptional activation also requires a similar duration of stimulation[2]. To keep NFAT in the nucleus, chronic elevated Ca^{2+} levels for at least 4 h of depolarization are required for reporter expression in cortical and hippocampal neurons, as well as HEK293 cells[66,67]. In the future, it may be possible to achieve a shorter minimal treatment time by using higher acoustic intensity with a shorter ST, duty cycle, and pulse duration, but this requires further testing.

Finally, we demonstrated the stimulation of therapeutic cellular devices in deep tissues. Given that the tissue attenuates ultrasound signal intensity, using a focused transducer or increasing acoustic intensity could enhance the stimulation effects. An alternative approach involves boosting mechanosensitivity through ectopic expression of mechanosensitive ion channels or the introduction of gas-filled vesicles, as seen in engineered T cells[25]. Engineered TFs that target DNA sequences different from the NFAT targeting domain offer clear advantages in terms of orthogonality and the ability to function without triggering the natural Ca^{2+}-dependent NFAT signaling pathways. One example is the utilization of endogenous NFAT signaling pathways to induce CAR expression, achieved by using microbubbles and introducing a Piezo1 mechanosensitive ion channel into Jurkat cells[25]. This method resulted in a minute 28% increase in relative CAR expression upon a 10-minute insonation period.

As a demonstration of potential therapeutic application, the therapeutic cellular device proved effective in mitigating acute DSS-induced murine colitis. Our sonogenetic approach demonstrated improvements in colon morphology and histopathology, showcasing a promising approach for targeted anti-inflammatory therapeutics.

In summary, the localized application of acoustic waves can effectively activate engineered cells that express an ultrasound-responsive switch, allowing the conversion of the acoustic signal into selected protein expression or other relevant output. The highly modular sonogenetic approach enables straightforward means to reconfigure the ultrasound switch for targeting the expression of any set of proteins. Moreover, achieving remote and locally confined activation within deep tissue holds significant importance for minimizing the potential side effects of various therapeutic interventions. This capability can be to tune the activation of therapeutic cells to e.g., suppress inflammation[58] or promote T-cell homing for solid tumors[28,29]. Future work should address current limitations such as reduction of peak Ca^{2+} amplitudes with repeated stimulations, possible

desensitization of ion channels, and incomplete release of transcription factors. Potential improvements include optimizing ultrasound parameters for sustained Ca^{2+} influx, exploring higher sound intensity for deeper tissue stimulation, using gas-filled vesicles or mechanosensors, and refining the delivery of therapeutic proteins. While a calcium-dependent signaling pathway offers the advantage of signal amplification, it may not be applicable to all cell types, especially those that regulate various functions via calcium signaling. While HEK293 cells served as a valuable proof of concept for their response to ultrasound, viability, metabolic activity, and other parameters should be evaluated individually for each cell line. Factors such as the sensitivity of certain cell types, e.g., neurons and cardiomyocytes, to ultrasound stimulation may require adjustments to achieve optimal results. Therefore, it is important to evaluate and adjust parameters on a case-by-case basis to ensure the safety and efficacy of ultrasound-mediated cell activation in different cell types.

Despite challenges, our work has demonstrated the ability of low-intensity pulsed ultrasound to modulate cellular activity and penetrate deep tissue, providing a promising foundation for the development of precision medicine in advanced therapies.

Methods

Animals

All animal experiments adhered to the EU 2010/63 directives and were approved by the Administration of the Republic of Slovenia for Food Safety, Veterinary Sector and Plant Protection of the Ministry of Agriculture, Forestry and Foods, Republic of Slovenia (Permit Number U34401-12/2018/13, U34401-25/2023/9).

BALB/c OlaHsd and Hsd:ICR (CD-1) mice were purchased from Envigo (Italy). Eight to thirteen-week-old male and female mice were used for the experiments.

Laboratory animals were housed in IVC cages GM500 (Techniplast), fed standard chow (Mucedola), and unrestricted access to tap water was provided. The cages were enriched using Nestlets nesting material and mouse houses. The mice were maintained in a controlled environment with a 12:12-hour dark/light cycle, relative humidity ranging from 40% to 60%, and an ambient temperature of 22 °C. All animals, used in the study were in good health, accompanied by a health certificate from the animal vendor. Health and microbiological statuses were confirmed by the Federation of European Laboratory Animal Science Associations recommended Mouse Vivum immunocompetent panel (QM Diagnostics).

Cell cultures

Human HEK293 and HEK293T (ATCC, CRL-1573, and CRL-3216) embryonic kidney cell lines were cultured in complete media (DMEM; 1 g l^{-1} glucose, 10% heat-inactivated FBS (Gibco, Invitrogen)) in a 5% CO_2 at 37 °C. In experiments with $GdCl_3$, Dulbecco's modified Eagle's medium without phosphate (DMEM; Invitrogen) supplemented with 10% fetal bovine serum (Gibco) was used. The Jurkat cell line (ATCC, TIB-152) was cultured in RPMI (Gibco, Invitrogen) supplemented with 10% (v/v) heat-inactivated FBS (Gibco, Invitrogen) in 5% CO_2 at 37 °C.

Plasmids

Plasmids $hNFAT^{FL}$:BFP, $mNFAT^{462}$:$TALE^{\Delta NLS}$:VP16:KRφ (expressing NFAT:TALE:VP16:KRφ) and $mNFAT^{462}$:$TALE^{\Delta NLS}$:VP16 (expressing NFAT:TALE:VP16) were constructed using the Gibson assembly method[68], and their amino acid sequences are listed in Supplementary Table 7. Plasmid expressing human $NFAT^{FL}$, mouse $NFAT^{FL}$, plasmid encoding firefly luciferase under $_{3\times NFAT}P_{IL2}$ promoter, and human interleukin-10 (hIL-10) were obtained from Addgene (id. no. 24219, 11791, 17870, 85430). Plasmids phRL-TK constitutively expressing *Renilla* luciferase for the normalization of transfection efficiency and pGL4.32[luc2P/NF-κB-RE/Hygro] containing five copies of an NF-κB response element that drives transcription of the luciferase reporter gene for testing NF-κB response were obtained from Promega. Plasmid pCRE-Luc containing cAMP response elements (CRE) that drive transcription of the luciferase reporter gene for testing CREB response was obtained from BD Clontech. The plasmids $mNFAT^{462}$:TALE:VP64 (expressing NFAT:TALE:VP64), $mNFAT^{462}$:TALE:VP64:KRφ (expressing NFAT:TALE:VP64:KRφ), $_{3\times NFAT}P_{min}$_fLuc, $_{10TALE}P_{min}$_fLuc, and $_{10TALE}P_{min}$_hIL-10 with sequences were described previously[36].

Ultrasound signal generator MODUSON-2

Ultrasound signal generator MODUSON-2 coupled with a 100 W RF power amplifier (2100 L, 100 W, 10 kHz-12 MHz; Electronics & Innovation, Ltd.) for pulsed cell stimulation, can deliver a wide range and shapes of stimulation signals to stimulate cells cultivated in petri-dish and to stimulate cells embedded in animal tissues. TA dedicated Wi-Fi-controlled measurement card Red Pitaya, based on a Linux system, acting as an embedded computer was used to control ultrasound parameters. Modern programming tools JavaScript, C++, and HTML compatible with MATLAB through so-called SCPI commands were used to program and control MODUSON-2. The signal is then fed back into MODUSON-2 for impedance matching and voltage increase up to 1 kV_{pp} and then to the ultrasonic transducer.

Calculating ultrasound pressure

The output pressures were measured using a calibrated needle hydrophone (NH0500, Precision Acoustics Ltd) connected to a pre-amplifier and a DC Coupler (Precision Acoustics Ltd). The hydrophone measurements were performed in a water tank at distances of 1 to 25 mm from the transducer's face. When converting the measured voltages into pressures, we accounted for the hydrophone capacitance according to the manufacturer's calibration. Using the appropriate conversion factor identified from the hydrophone's calibration data that was supplied with the hydrophone, the hydrophone voltage-trace waveform was transformed into an acoustic-pressure waveform measured in MPa.

Ultrasound stimulation for cell cultures

For fluorescence imaging of Ca^{2+} influx while performing simultaneous ultrasonic stimulation a confocal microscope (SP5, Leica) was used. A 3.5-cm glass bottom dish (Cellvis) or 6-well glass bottom plate (Cellvis) containing HEK293 or Jurkat cells loaded with a Ca^{2+}-sensitive dye was placed on the stage of an inverted microscope and a 0.5 MHz ultrasound transducer (Olympus V318-SU) was carefully lowered into the media from the top. The ratiometric Ca^{2+}-sensitive dyes Fluo4 (Biotium) and FuraRed (Setareh Biotech) or CalRed (AAT Bioquest) were used for imaging changes in intracellular Ca^{2+} concentration.

For ultrasound stimulation, HEK293 or Jurkat cells were seeded in 3.5-cm glass bottom dishes. The cells were treated with ultrasound using a 0.5 MHz transducer (Olympus V318-SU) positioned below the petri dish. A 3D-printed plastic holder was used to secure the transducer and petri dish in place. All ultrasound stimulations were conducted using parameters including a 0.31 MHz frequency, with pulse repetition frequency (PRF) of 1 kHz, duty cycle (DC) of 32%, 10 s stimulation time (ST), 110 s resting period and 2 h treatment time (TT), unless stated otherwise.

Pharmacological treatments

Chemical blockers and peptide inhibitors (all from MedChemExpress) were employed to directly target ion channels or modulate cellular pathways. Control samples received equivalent volumes of buffer solutions. Gadolinium, at a final concentration of 0.4 mM, was utilized to non-specifically inhibit mechanosensitive ion channels. Ruthenium red (IC_{50}~ 500 nM, 1 μM), TTA-P2 (IC_{50}~ 22 nM, 3 μM) and Pico145 (IC_{50}~ 1.3 nM, 5 nM) were administered one hour before ultrasound stimulation to respectively block TRP channels (TRPV1, 2, 4), T-type calcium channels and TRPC1, TRPC4 and TRPC5 channels. To inhibit G

protein-coupled receptors (GPCRs), suramin (IC_{50}~ 200 nM, 60 µM) was introduced into the medium and incubated with cells for one hour prior to ultrasound stimulation. Lastly, GsMTx4 (IC_{50}~ 5 µM, 10 µM) was included in the medium and incubated with cells for two hours to inhibit Piezo1 channel gating and then stimulated with ultrasound.

Ultrasound stimulation in vivo

In vivo experiments were performed on BALB/c OlaHsd mice. The suspension of transfected HEK293T cells (2×10^6 cells in 150 µl PBS) was injected subcutaneously into the indicated hind limb of the mice. On the day of injection, the mice were anesthetized with 1.8% MAK isoflurane anesthesia (Harvard Apparatus, Holliston, MA, USA) and maintained at 37 °C using a surgical heating pad. All ultrasound stimulations were carried out using a 0.5 MHz transducer (Olympus V318-SU) with parameters – 0.31 MHz frequency, 1 kHz PRF, 32% DC, 10 s ST, 110 s resting period, and 2 h TT unless stated otherwise. After 4 h, mice received 150 mg kg^{-1} of body weight of D-luciferin (Xenogen) subcutaneously and were in vivo imaged using IVIS Lumina Series III (PerkinElmer). The data was analyzed using Living Image 4.5.2 (PerkinElmer).

For deep tissue stimulation, the suspension of 4×10^6 transfected HEK293T cells in 500 µl ECM Gel from Engelbreth-Holm-Swarm murine sarcoma (Sigma Aldrich) was implanted i.p. in mice. The following day, the mice were anesthetized with 1.8% MAK isoflurane anesthesia (Harvard Apparatus, Holliston, MA, USA) and maintained at 37 °C using a surgical heating pad. Ultrasound stimulation was performed using the same parameters as mentioned above. After 6 h, the presence of iRFP was determined through fluorescent signal analysis, with spectral unmixing performed to eliminate tissue autofluorescence. Following fluorescence imaging, the mice received 150 mg kg^{-1} of body weight of D-luciferin (Xenogen) intraperitoneally and were in vivo imaged after 10-15 min using IVIS Lumina Series III (PerkinElmer). The data was analyzed using Living Image 4.5.2 (PerkinElmer). Constitutively expressed iRFP was used as a transfection efficiency control and for visualizing localized stimulation. The luminescence intensity of fLuc was normalized to the fluorescence intensity of iRFP in the region of interest.

Therapeutic cellular device preparation

For the preparation of the cell device, modified polyvinylidene difluoride (mPVDF) hollow fibers KrosFlo Implant Membranes with 500 kDa (20 nm) pores and 1 mm diameter (Spectrum Labs) were used. The mPVDF membranes selected for our study have been proven by the manufacturer to be biocompatible in various animal models for periods exceeding 14 days. Furthermore, according to the manufacturer, the cell lines grown in the KrosFlo implant membranes, as used in our experiment, are not susceptible to immunological attack by the host animal[69–71]. Cell encapsulation was performed as described in ref. 55. Briefly, the hollow fiber was filled with transfected HEK293T (for the therapeutic cellular device) or wild-type HEK293T cells (for the sham device) at a concentration of 4.2×10^6 cells ml^{-1} and heat-sealed in 1–1.2 cm long segments (~ 3.3×10^4 cells/device). The therapeutic cellular device was used for in vitro and in vivo experiments.

Evaluation of therapeutic cellular device in vitro

The therapeutic devices were prepared as described in **Therapeutic cellular device preparation**. The devices were incubated in a 3.5-cm glass bottom petri dish (Cellvis), with six devices per dish. Subsequently, the devices underwent stimulation for 2 h per day, spanning two consecutive days. ELISA samples were collected each day, 6 h after stimulation. On the third day, following ELISA sample collection, cells were flushed from the hollow fibers and viability was measured using trypan blue dye and cell counter Countess™ (Invitrogen). Ultrasound stimulations were performed using a 1 MHz transducer (TX_1_19, Precision Acoustics, Dorchester, UK) with the sequence: 1 MHz frequency, 1 kHz PRF, 10% DC, 10 s ST, and 110 s resting period.

Animal model of acute colitis

Animal model experiments were performed on Hsd:ICR (CD-1) mice. For the experiments, 35 mice were randomly allocated into seven groups. Three mice were excluded due to post-operational complications, and specific group sizes are indicated in the figure captions.

The application of the therapeutic cellular device in vivo was demonstrated in an acute murine colitis model[72]. The therapeutic and sham cellular devices were prepared as described in **Therapeutic cellular device preparation**. The mice were given either water or 4% (w/v) DSS (TdB Consultancy, DB001-31) solution for 9 days, and on the third day (Fig. 4B) of this time-course experimental model, six therapeutic cellular devices per mouse were surgically implanted into the abdomen under general inhalation isoflurane anesthesia, 1.8% MAK (Harvard Apparatus, Holliston, MA, USA). Analgesia was provided by meloxicam (2 mg/kg) injection (Boehringer Ingelheim, Ingelheim, Germany). Control groups without engineered cells received a sham device (encapsulated wild-type HEK293T cells). The next day, mice were anesthetized with 1.8% MAK isoflurane anesthesia (Harvard Apparatus, Holliston, MA, USA) and maintained at 37 °C using a surgical heating pad. Two-hour ultrasound stimulation was carried out on days 4, 5, and 6 using a 1 MHz transducer (TX_1_19, Precision Acoustics, Dorchester, UK) with the sequence: 1 MHz frequency, 1 kHz PRF, and 10% DC, 10 s ST and 110 s resting period. The human recombinant IL-10 group received 2.5 ng of hrIL-10 (Gibco, 200-10-2UG) i.p. on days 4, 5, and 6. Weight was monitored daily; stool blood and stool consistency were determined on the last day. The disease activity index (DAI) was determined by combining the stool blood and stool consistency scores. Each score was determined as follows: stool blood, 0–2 (0, no blood; 1, hemoccult bleeding; 2, gross bleeding); and stool consistency, 0–2 (0, normal stool; 1, soft stool; 2, diarrhea). Colon length was measured post-sacrifice, from the body of the cecum to the distal part of the rectum. The histological score was determined as previously described: formation of ulcus, 0–4; epithelium morphology, 0–4; immune cell infiltration, 0–4; and lymph follicles, 0–4[73].

Tissue staining

Histological samples of the sacrificed mice were fixated overnight in 10% neutral buffered formalin (Sigma-Aldrich; HT501128) and then embedded in paraffin (Leica; Paraplast; 39601006). The paraffin blocks were cut 7 µm thick with a rotation microtome RM 2245 (Leica; 1492245UL01). The tissue sections underwent deparaffinization and rehydration using xylene and different dilutions of ethanol (Sigma Aldrich). The tissue samples were then mounted on slides using a Leica CV Mount (Leica) and stained with hematoxylin and eosin (Sigma-Aldrich; MHS32; HT110332) according to the manufacturer's protocol.

In vivo plasmid electroporation

In vivo experiments were conducted on BALB/c OlaHsd mice. Plasmid DNA, 30 µg in a final volume of 30 µL PBS, was injected into the indicated hind limb muscle, followed by electroporation using the Gene Pulser Xcell Total Electroporation System (Bio-Rad Laboratories) with SonidelTM round 5-mm electrodes (CUY650P5). Electroporation parameters were set as follows: Voltage 900, pulse width 100 µs, pulse interval 1 s, and pulse number 5. Post-electroporation analgesia was provided by a meloxicam injection (2 mg kg^{-1}, Boehringer Ingelheim, Ingelheim, Germany).

The following day, mice were anesthetized with 1.8% MAK isoflurane anesthesia (Harvard Apparatus, Holliston, MA, USA) and maintained at 37 °C using a surgical heating pad. Two-hour ultrasound stimulations were carried out.

For luciferase experiments, mice received a subcutaneous injection of 150 mg kg^{-1} D-luciferin (Xenogen) 4 hours after stimulation and

were imaged in vivo using IVIS Lumina Series III (PerkinElmer). Data analysis was performed using Living Image 4.5.2 (PerkinElmer).

In hIL-10 experiments, mice were sacrificed 4 hours after stimulation via cervical dislocation, and hind leg muscles were harvested. Muscles were homogenized on ice in Passive lysis buffer (Promega) supplemented with a protease inhibitor cocktail (P8340, Sigma-Aldrich) using a mechanical tissue homogenizer. Homogenates were then centrifuged at 13,000 g for 15 minutes at 4 °C, and the supernatant was collected. Human IL-10 levels were quantified using ELISA (Invitrogen) and normalized by total protein content determined through a Pierce BCA Protein Assay (Thermo Scientific).

Mammalian cell viability assay

HEK293 cells, both transfected and wild-type, were cultured in a 3.5-cm glass bottom petri dish (Cellvis) or 6-well glass bottom plate (Cellvis). Ultrasound stimulation was applied from the top (for Ca^{2+} imaging) or bottom using a 0.5 MHz transducer (Olympus V318-SU). The bottom of the plate was acoustically coupled to the transducer using coupling gel. Following ultrasound stimulation, cells were returned to the incubator for 24 hours. Viability was assayed using 7-AAD viability dye (Invitrogen) following the manufacturer's protocol, comparing ultrasound-stimulated cells to non-insonated control cells. Cell death was measured using a spectral flow cytometer (Aurora, Cytek Biosciences). For assessing metabolic activity, an MTT assay was used. Following treatment with ultrasound in a 3.5-cm glass-bottom petri dish, the cells were harvested using trypsin, resuspended in serum-free media, and transferred to a 96-well plate for MTT assay following the manufacturer's protocol (M5655, Sigma-Aldrich).

Transfection, electroporation, and stimulation

For dual luciferase assays and ELISA, 2×10^4 HEK293T cells were seeded per well in 96-well plates (Corning). For confocal microscopy experiments, 3×10^4 HEK293 cells were seeded per well in an 8-well chamber slide (Ibidi). For ultrasound stimulation experiments, 8×10^5 HEK293 cells were seeded per well in 6-well glass bottom plates (Cellvis) or a 3.5-cm glass bottom petri dish (Cellvis). At 50–70% confluence, HEK293 cells were transfected with a mixture of DNA and polyethyleneimine (PEI, linear, Mw 25000; Polysciences, catalog no. 23966). Per 500 ng DNA, 6 μl of PEI stock solution (0.324 mg ml^{-1}, pH 7.5) was used.

Jurkat cells (3×10^7 cells ml^{-1}) were electroporated by Neon electroporation system (Thermo Fisher Scientific), using R buffer in 100 μl electroporation tips (electroporation parameters: 1600 V voltage, 10 ms pulse width, 3 pulses). After electroporation, the cells were resuspended in 2 ml of fresh medium.

Twenty-four hours after transfection or electroporation, the culture medium was replaced with a fresh medium, and the cells were stimulated with ultrasound or the indicated concentration of ionophore (Ca^{2+} ionophore A23187, Sigma Aldrich) or cyclosporine A (BioVision), for the indicated times. Ca^{2+} ionophore A23187 was prepared as a 10 mM stock solution in DMSO, and cyclosporine A as a 25 mM stock solution in DMSO. "No stimulation - NS" or "buffer" means incubation with the solvent used for the stock solution in the experiment.

In experiments where cyclosporine A was used in combination with ultrasound or ionophore, cells were pre-incubated with 1 μM or 10 μM cyclosporine A for 30 min before stimulation with ultrasound or ionophore, respectively.

The amounts of transfected plasmids are indicated in the figures and figure captions or presented in Supplementary Tables 1–6. The phRL-TK plasmid (Promega), encoding the *Renilla* luciferase, was used as a transfection efficiency control in luciferase experiments. The empty pcDNA3 plasmid (Invitrogen) was used to equalize the total DNA amounts over different experimental conditions.

Luciferase reporter assay

Cells were lysed at the indicated time points using 25 μl of 1 × Passive lysis buffer (Promega) per well. Firefly luciferase (fLuc) and *Renilla* luciferase (rLuc) activities were measured using the dual luciferase assay (Promega) on an Orion II microplate reader (Berthold Technologies). Relative luciferase units (RLUs) were calculated by normalizing fLuc to the constitutive rLuc in each sample. Normalized RLU (nRLU) values were calculated by normalizing the RLU values of each sample to the average RLU value of the unstimulated reporter-only samples within the same experiment.

Immunostaining

For immunofluorescent analysis of protein localization, cells were fixed with 4% formaldehyde (Histofix, Roth) and permeabilized with 0.1% Triton X-100 (Thermo Scientific) after stimulation. The cells were stained with anti-Myc tag rabbit polyclonal primary antibodies (C3956, Sigma-Aldrich) at a dilution of 1:100 and then incubated with Alexa Fluor 647-conjugated goat antirabbit IgG secondary antibodies at a dilution of 1:2000 (A-21246, Invitrogen); 300 nM DAPI (Invitrogen) was used as a nuclear stain. During microscopy, the cells were kept in a chamber at 37 °C. To maintain the physiological pH, 10 mM HEPES pH 7.4 (from 1 M stock solution) was added to the media. Confocal images were obtained.

Confocal imaging analysis

To evaluate the nuclear translocation of $hNFAT^{FL}$, BFP-fused constructs were transfected into HEK293T cells. HEK293T cells were seeded onto 8-well tissue culture chambers (Ibidi) at 3×10^4 cells per well, respectively. Twenty-four hours post-transfection, the cells were incubated for 2 h in either medium (unstimulated) or were subjected to stimulation with ultrasound or 5 μM ionophore (Ca^{2+} ionophore A23187, Sigma Aldrich). Leica LAS AF software was used for acquisition, and ImageJ software (National Institute of Mental Health, Bethesda, USA) was used for image processing.

Microscopic images were obtained using a Leica TCS SP5 inverted laser-scanning microscope on a Leica DMI 6000 CS module equipped with an HCX Plan-Apochromat lambda blue 63× objective, numerical aperture 1.4 (Leica Microsystems). A 50-mW 405 nm diode laser was used for BFP and DAPI excitation (emission between 420 and 460 nm). A 10-mW 633 nm HeNe laser was used for Alexa Fluor 647 excitation (emission between 650 and 690 nm).

A 65-mW 488 nm Argon laser was used for the excitation of Ca^{2+}-sensitive ratiometric dyes - a combination of Fluo-4 and FuraRed, or CalRed. An increase in fluorescence emission intensity at 515 nm upon Ca^{2+} binding (525 nm for CalRed) with a decrease of fluorescence emission at 655 nm of FuraRed (650 nm for CalRed) was followed over time. The ratio of fluorescence emission intensities was calculated for selected regions of interest. Individual cells were selected using an ImageJ macro which selected cells based on labeled nuclei. The ROI overlapped the 525-nm channel and the 650-nm channel to extract changes in the intensities of individual cells (Supplementary Fig. 12).

The FI ratios, normalized to the average FI ratio prior to stimulation, have been plotted as heatmaps for the cells shown. The pre-stimulation averaged FI ratios were used as a baseline to calculate the area under the curve for the response to stimulation. Calcium signals within a time window between 0 s (start of ultrasound) and 120 s were used to calculate the area under the curve.

Immunoblotting

One day after seeding, the cells were stimulated for two hours with ultrasound or for 30 min with sorbitol (0.4 M, S-6021, Sigma-Aldrich) (positive control). After stimulation, stimulated and unstimulated cells were washed with 1 ml of PBS and lysed in 100 μl of 1 × Passive lysis buffer (Promega), supplemented with complete protease inhibitor cocktail (P8340, Sigma-Aldrich) and phosphatase inhibitor cocktail 2

(P5726, Sigma-Aldrich). The protein concentration in each sample was determined with a Pierce BCA Protein Assay (Thermo Scientific) following the manufacturer's instructions. Absorbance at 562 nm was measured on a Synergy Mx automated microplate reader (BioTek) using Gen5 software. Samples (50 µg of total protein per sample) were separated by SDS-PAGE (200 V, 10% polyacrylamide gel) and transferred to a nitrocellulose membrane using iBlot 2 Dry Blotting System (Thermo Fisher Scientific) according to the manufacturer's protocol. The membrane was incubated with phospho-p38 MAPK (Thr180/Tyr182) primary antibodies (1:1000, Cell Signaling Technology, #9211) and anti-PCNA primary antibodies (1:1000, Abcam, ab29) and secondary antibodies (1:2000, goat antirabbit IgG-HRP Abcam, ab6721; and 1:2000, goat anti-mouse IgG-HRP, Jackson Immuno Research, 115-035-003). Membrane blocking, antibody binding, and membrane washing were performed with an iBind Flex Western Device (Thermo Fisher Scientific) according to the manufacturer's protocol. The immunoblots were visualized in a G-box analyzer (Syngene) after they were developed using the Femto Sensitivity substrate (Thermo Fisher Scientific). ImageJ software (National Institute of Mental Health, Bethesda, USA) was used for image processing.

ELISA

For the detection of hIL-10, supernatant or mouse serum was collected at indicated time points and used for ELISA (IL-10 Human Uncoated ELISA kit, 88-7106-77, Thermo Scientific). The impact of ultrasound on inflammation in mice was monitored following the expression of mIL-1β, mIL-6 and mTNF-α. Levels were assessed in serum 24 h after insonation using corresponding ELISA kits (IL-1β Mouse Uncoated ELISA kit, 88-7013-88; IL-6 Mouse Uncoated ELISA kit, 88-7064-88; TNF-α Mouse Uncoated ELISA kit, 88-7324-88, Thermo Scientific).

To assess the impact of ultrasound on native NFAT activation in wild-type Jurkat cells, the expression of hIL-2 and hTNF-α was monitored in the cell supernatant 24 h after insonation using the relevant ELISA kits (IL-2 Human Uncoated ELISA kit, 88-7025-77; TNF-α Human Uncoated ELISA kit 88-7346-88, Thermo Scientific). The ELISA assays were conducted following the manufacturer's instructions, using appropriate dilutions. Absorbance was measured using a Synergy Mx automated microplate reader (BioTek) at 450 nm and 630 nm using Gen5 software. Absorbance at 630 nm was used for correction and was subtracted from the absorbance at 450 nm.

Statistics & reproducibility

Graphs were prepared with Origin 8.1 (OriginLab Corporation, Northampton, MA, USA), and GraphPad Prism 6 (GraphPad Software, Boston, Massachusetts USA). All statistical analyses were performed with GraphPad Prism 6 and are presented as mean ± SD or SEM (Statistics are depicted in Supplementary Data 1 and in figure legends). The paired two-tailed t-test between two groups or one-way analysis of variance (ANOVA) with Tukey's multiple comparisons post-hoc test among three or more groups was used for comparisons. $P < 0.05$ is considered statistically significant. No statistical method was used to predetermine sample size; the sample size was chosen based on the published literature, depending on the technique used, and based on our experience. No power calculations were performed to choose group size. No data was excluded from the analysis. Independent biological replicates were performed to ensure the reproducibility of the results. All experiments were repeated in triplicate or more unless otherwise stated. Replicates are reported in the figures. All groups for cell imaging and ultrasound stimulation were randomized. Mice were randomly divided into different treatment groups. In a bilateral implantation experiment where both sides were implanted with cells and only one side received ultrasound treatment, that side was randomly determined to be the right side. The Investigators were not blinded during the experiments or analysis except for histological analysis. Blinding was not feasible in cases when the person performing the experiment and analyzing data was the same person. Blinding was performed when analyzing histological data, the person analyzing the histological slides was not aware of the group type.

Reporting summary

Further information on research design is available in the Nature Portfolio Reporting Summary linked to this article.

Data availability

The authors declare that the data supporting the findings of this study are available within the paper and its supplementary information files. Source data are provided in this paper.

Code availability

ImageJ macro with description is available in Supplementary Software 1 file.

References

1. Zhu, D., Johnson, H. J., Chen, J. & Schaffer, D. V. Optogenetic application to investigating cell behavior and neurological disease. *Front. Cell. Neurosci.* **16**, 811493 (2022).
2. Hannanta-anan, P. & Chow, B. Y. Optogenetic control of calcium oscillation waveform defines NFAT as an integrator of calcium load. *Cell Syst* **2**, 283–288 (2016).
3. Li, L. et al. Colocalized, bidirectional optogenetic modulations in freely behaving mice with a wireless dual-color optoelectronic probe. *Nat. Commun.* **13**, 839 (2022).
4. Tan, P., He, L., Han, G. & Zhou, Y. Optogenetic immunomodulation: Shedding light on antitumor immunity. *Trends Biotechnol.* **35**, 215–226 (2017).
5. Zhao, B. et al. An optogenetic controllable T cell system for hepatocellular carcinoma immunotherapy. *Theranostics* **9**, 1837–1850 (2019).
6. Nguyen, N. T., He, L., Martinez-Moczygemba, M., Huang, Y. & Zhou, Y. Rewiring calcium signaling for precise transcriptional reprogramming. *ACS Synth. Biol.* **7**, 814–821 (2018).
7. Rabut, C. et al. Ultrasound technologies for imaging and modulating neural activity. *Neuron* **108**, 93–110 (2020).
8. Tufail, Y., Yoshihiro, A., Pati, S., Li, M. M. & Tyler, W. J. Ultrasonic neuromodulation by brain stimulation with transcranial ultrasound. *Nat. Protoc.* **6**, 1453–1470 (2011).
9. Chen, M. et al. Numerical and experimental evaluation of low-intensity transcranial focused ultrasound wave propagation using human skulls for brain neuromodulation. *Med. Phys.* **50**, 38–49 (2023).
10. Carovac, A., Smajlovic, F. & Junuzovic, D. Application of ultrasound in medicine. *Acta Inform. Med.* **19**, 168–171 (2011).
11. Maresca, D. et al. Biomolecular ultrasound and sonogenetics. *Annu. Rev. Chem. Biomol. Eng.* **9**, 229–252 (2018).
12. Errico, C. et al. Ultrafast ultrasound localization microscopy for deep super-resolution vascular imaging. *Nature* **527**, 499–502 (2015).
13. King, R. L., Brown, J. R., Newsome, W. T. & Pauly, K. B. Effective parameters for ultrasound-induced in vivo neurostimulation. *Ultrasound Med. Biol.* **39**, 312–331 (2013).
14. Menz, M. D., Oralkan, O., Khuri-Yakub, P. T. & Baccus, S. A. Precise neural stimulation in the retina using focused ultrasound. *J. Neurosci.* **33**, 4550–4560 (2013).
15. Deffieux, T. et al. Low-intensity focused ultrasound modulates monkey visuomotor behavior. *Curr. Biol.* **23**, 2430–2433 (2013).
16. Hou, X. et al. Precise ultrasound neuromodulation in a deep brain region using nano gas vesicles as actuators. *Adv. Sci.* **8**, 2101934 (2021).
17. Liu, T. et al. Sonogenetics: Recent advances and future directions. *Brain Stimul.* **15**, 1308–1317 (2022).

18. Krasovitski, B., Frenkel, V., Shoham, S. & Kimmel, E. Intramembrane cavitation as a unifying mechanism for ultrasound-induced bioeffects. *Proc. Natl. Acad. Sci. USA* **108**, 3258–3263 (2011).
19. Plaksin, M., Kimmel, E. & Shoham, S. Cell-type-selective effects of intramembrane cavitation as a unifying theoretical framework for ultrasonic neuromodulation. *eNeuro* **3**, ENEURO.0136–15 (2016).
20. Kubanek, J., Shukla, P., Das, A., Baccus, S. A. & Goodman, M. B. Ultrasound elicits behavioral responses through mechanical effects on neurons and ion channels in a simple nervous system. *J. Neurosci.* **38**, 3081–3091 (2018).
21. Liao, D., Li, F., Lu, D. & Zhong, P. Activation of Piezo1 mechanosensitive ion channel in HEK293T cells by 30 MHz vertically deployed surface acoustic waves. *Biochem. Biophys. Res. Commun.* **518**, 541–547 (2019).
22. Duque, M. et al. Sonogenetic control of mammalian cells using exogenous transient receptor potential A1 channels. *Nat. Commun.* **13**, 600 (2022).
23. Yoo, S., Mittelstein, D. R., Hurt, R. C., Lacroix, J. & Shapiro, M. G. Focused ultrasound excites cortical neurons via mechanosensitive calcium accumulation and ion channel amplification. *Nat. Commun.* **13**, 493 (2022).
24. Szablowski, J. O., Bar-Zion, A. & Shapiro, M. G. Achieving spatial and molecular specificity with ultrasound-targeted biomolecular nanotherapeutics. *Acc. Chem. Res.* **52**, 2427–2434 (2019).
25. Pan, Y. et al. Mechanogenetics for the remote and noninvasive control of cancer immunotherapy. *Proc. Natl. Acad. Sci. USA* **115**, 992–997 (2018).
26. Abedi, M. H. et al. Ultrasound-controllable engineered bacteria for cancer immunotherapy. *Nat. Commun.* **13**, (2022).
27. Chen, Y., Du, M., Yuan, Z., Chen, Z. & Yan, F. Spatiotemporal control of engineered bacteria to express interferon-γ by focused ultrasound for tumor immunotherapy. *Nat. Commun.* **13**, 1–15 (2022).
28. Wu, Y. et al. Control of the activity of CAR-T cells within tumours via focused ultrasound. *Nat. Biomed. Eng.* **5**, 1336–1347 (2021).
29. Chen, X. et al. Non-invasive activation of intratumoural gene editing for improved adoptive T-cell therapy in solid tumours. *Nat. Nanotechnol.* **18**, 933–944 (2023).
30. Liu, P. et al. Sonogenetic control of multiplexed genome regulation and base editing. *Nat. Commun.* **14**, 6575 (2023).
31. Dewhirst, M. W. et al. Basic principles of thermal dosimetry and thermal thresholds for tissue damage from hyperthermia. *Int. J. Hyperth.* **19**, 267–294 (2003).
32. McDannold, N. J., King, R. L., Jolesz, F. A. & Hynynen, K. H. Usefulness of MR imaging-derived thermometry and dosimetry in determining the threshold for tissue damage induced by thermal surgery in rabbits1. *Radiology* **216**, 517–523 (2000).
33. McDannold, N., Vykhodtseva, N., Jolesz, F. A. & Hynynen, K. MRI investigation of the threshold for thermally induced blood–brain barrier disruption and brain tissue damage in the rabbit brain. *Magn. Reson. Med.* **51**, 913–923 (2004).
34. Tufail, Y. et al. Transcranial pulsed ultrasound stimulates intact brain circuits. *Neuron* **66**, 681–694 (2010).
35. Chu, Y.-S. Y.-C. et al. Elevation of intra-cellular calcium in nucleus pulposus cells with micro-pipette-guided ultrasound. *Ultrasound Med. Biol.* **47**, 1775–1784 (2021).
36. Meško, M., Lebar, T., Dekleva, P., Jerala, R. & Benčina, M. Engineering and rewiring of a calcium-dependent signaling pathway. *ACS Synth. Biol.* **9**, 2055–2065 (2020).
37. Zhang, J., Yuan, H., Yao, X. & Chen, S. Endogenous ion channels expressed in human embryonic kidney (HEK-293) cells. *Pflügers Arch. - Eur. J. Physiol.* **474**, 665–680 (2022).
38. Gnanasambandam, R. et al. GsMTx4: Mechanism of inhibiting mechanosensitive ion channels. *Biophys. J.* **112**, 31 (2017).
39. Vriens, J., Appendino, G. & Nilius, B. Pharmacology of vanilloid transient receptor potential cation channels. *Mol. Pharmacol.* **75**, 1262–1279 (2009).
40. Rubaiy, H. N. et al. Picomolar, selective, and subtype-specific small-molecule inhibition of TRPC1/4 /5 channels. *J. Biol. Chem.* **292**, 8158–8173 (2017).
41. Choe, W. J. et al. TTA-P2 Is a potent and selective blocker of T-type calcium channels in rat sensory neurons and a novel antinociceptive agent. *Mol. Pharmacol.* **80**, 900 (2011).
42. Freissmuth, M. et al. Suramin analogues as subtype-selective G protein inhibitors. *Mol. Pharmacol.* **49**, 602–611 (1996).
43. Hogan, P. G., Chen, L., Nardone, J. & Rao, A. Transcriptional regulation by calcium, calcineurin, and NFAT. *Genes Dev* **17**, 2205–2232 (2003).
44. Kim, E.-J. & Kim, G.-Y. Effect of low intensity pulsed ultrasound in activating the mitogen-activated protein kinase signaling pathway and inhibition inflammation cytokine synthesis in chondrocytes. *Phys. Ther. Rehabil. Sci.* **3**, 33–37 (2014).
45. Fisher, W. G., Yang, P. C., Medikonduri, R. K. & Jafri, M. S. NFAT and NFκB activation in T lymphocytes: A model of differential activation of gene expression. *Ann. Biomed. Eng.* **34**, 1712–1728 (2006).
46. Wang, H., Xu, J., Lazarovici, P., Quirion, R. & Zheng, W. cAMP Response element-binding protein (CREB): A possible signaling molecule link in the pathophysiology of schizophrenia. *Front. Mol. Neurosci.* **11**, 382173 (2018).
47. Yeung, T. et al. Receptor activation alters inner surface potential during phagocytosis. *Science* **313**, 347–351 (2006).
48. Yeung, T. et al. Membrane phosphatidylserine regulates surface charge and protein localization. *Science* **319**, 210–213 (2008).
49. Roy, M.-O., Leventis, R. & Silvius, J. R. Mutational and biochemical analysis of plasma membrane targeting mediated by the farnesylated, polybasic carboxy terminus of K-ras4B. *Biochemistry* **39**, 8298–8307 (2000).
50. Lee, W., Weisholtz, D. S., Strangman, G. E. & Yoo, S.-S. Safety review and perspectives of transcranial focused ultrasound brain stimulation. *Brain Neurorehabil.* **14**, e4 (2021).
51. Marketing Clearance of Diagnostic Ultrasound Systems and Transducers - Guidance for Industry and Food and Drug Administration Staff.
52. Moore, K. W., de Waal Malefyt, R., Coffman, R. L. & O'Garra, A. Interleukin-10 and the interleukin-10 receptor. *Annu. Rev. Immunol.* **19**, 683–765 (2001).
53. Kleiner, G., Marcuzzi, A., Zanin, V., Monasta, L. & Zauli, G. Cytokine levels in the serum of healthy subjects. *Mediators Inflamm.* **2013**, 434010 (2013).
54. Kohno, H., Suzuki, R., Sugie, S. & Tanaka, T. Suppression of colitis-related mouse colon carcinogenesis by a COX-2 inhibitor and PPAR ligands. *BMC Cancer* **5**, 1–12 (2005).
55. Kadunc Polajnar, L. et al. Engineered combinatorial cell device for wound healing and bone regeneration. *Front. Bioeng. Biotechnol.* **11**, 1168330 (2023).
56. Steidler, L. et al. Treatment of murine colitis by lactococcus lactis secreting interleukin-10. *Proc. Natl. Acad. Sci. USA* **76**, 104 (1994).
57. Sasaki, M. et al. Reversal of experimental colitis disease activity in mice following administration of an adenoviral IL-10 vector. *J. Inflamm.* **2**, 13 (2005).
58. Smole, A., Lainšček, D., Bezeljak, U., Horvat, S. & Jerala, R. A synthetic mammalian therapeutic gene circuit for sensing and suppressing inflammation. *Mol. Ther.* **25**, 102–119 (2017).
59. Tan, J. C., Indelicato, S. R., Narula, S. K., Zavodny, P. J. & Chou, C. C. Characterization of interleukin-10 receptors on human and mouse cells. *J. Biol. Chem.* **268**, 21053–21059 (1993).
60. Feng, C. G. et al. Transgenic mice expressing human interleukin-10 in the antigen-presenting cell compartment show increased susceptibility to infection with mycobacterium avium associated with

decreased macrophage effector function and apoptosis. *Infect. Immun.* **70**, 6672–6679 (2002).
61. Kichler, A., Leborgne, C., Coeytaux, E. & Danos, O. Polyethylenimine-mediated gene delivery: A mechanistic study. *J. Gene Med.* **3**, 135–144 (2001).
62. Oh, Y. K. et al. Polyethylenimine-mediated cellular uptake, nucleus trafficking and expression of cytokine plasmid DNA. *Gene Ther.* **9**, 1627–1632 (2002).
63. Wang, X., Wong, K., Ouyang, W. & Rutz, S. Targeting IL-10 family cytokines for the treatment of human diseases. *Cold Spring Harb. Perspect. Biol.* **11**, a028548 (2019).
64. van Deventer, S., Elson, C. & Fedorak, R. Multiple doses of intravenous interleukin 10 in steroid-refractory Crohn's disease. Crohn's disease study group. *Gastroenterology* **113**, 383–389 (1997).
65. Hao, J. & Delmas, P. Multiple desensitization mechanisms of mechanotransducer channels shape firing of mechanosensory neurons. *J. Neurosci.* **30**, 13384–13395 (2010).
66. Pont, J. N. A., McArdle, C. A. & López Bernal, A. Oxytocin-stimulated NFAT transcriptional activation in human myometrial cells. *Mol. Endocrinol.* **26**, 1743–1756 (2012).
67. Vihma, H., Luhakooder, M., Pruunsild, P. & Timmusk, T. Regulation of different human NFAT isoforms by neuronal activity. *J. Neurochem.* **137**, 394–408 (2016).
68. Gibson, D. D. G. et al. Enzymatic assembly of DNA molecules up to several hundred kilobases. *Nat. Methods* **6**, 343–345 (2009).
69. Casciari, J. J. et al. Growth and chemotherapeutic response of cells in a hollow-fiber in vitro solid tumor model. *J. Natl. Cancer Inst.* **86**, 1846–1852 (1994).
70. Hollingshead, M. G. et al. In vivo cultivation of tumor cells in hollow fibers. *Life Sci.* **57**, 131–141 (1995).
71. Hollingshead, M. et al. In vivo drug screening applications of HIV-infected cells cultivated within hollow fibers in two physiologic compartments of mice. *Antiviral Res.* **28**, 265–279 (1995).
72. Wirtz, S., Neufert, C., Weigmann, B. & Neurath, M. F. Chemically induced mouse models of intestinal inflammation. *Nat. Protoc.* **2**, 541–546 (2007).
73. Kojouharoff, G. et al. Neutralization of tumour necrosis factor (TNF) but not of IL-1 reduces inflammation in chronic dextran sulphate sodium-induced colitis in mice. *Clin. Exp. Immunol.* **107**, 353–358 (1997).

Acknowledgements

We thank the late Dejan Križaj, Faculty of Electrical Engineering, University of Ljubljana for his assistance and support in the early stages of the project. We thank Zumret Topcagić for constructing the wave generator. This research was supported by the Slovenian Research and Innovation Agency (research core funding nos. P4-0176 (R.J.), J1-4408 (M.B.), J4-1779 (M.B.), J3-9268 (M.B.)), an ONR grant (no. N629092012090 (M.B. and R.J.)), the ERC project MULTraSonicA (no. 885155 (M.B.)) and EU funding (no. 101059842 (M.B. and R.J.), CTGCT).

Author contributions

M.M., F.I., and T.L. designed and constructed plasmids expressing transcription factors and reporters. M.M. and F.I. planned and performed the ultrasound-stimulation experiments. M.G. provided initial advice on the ultrasound. M.R., F.I., and M.M. designed and analyzed the impact of ultrasound on Ca^{2+} influx. M.B. and R.J. conceived the project. M.B., F.I., and M.M. designed the experiments and analyzed the data. D.L. and F.I. planned, performed, and analyzed in vivo experiments. M.B. wrote the manuscript with input from all authors. All authors discussed the results and reviewed and contributed to the manuscript.

Competing interests

The authors declare no competing interests.

Additional information

Supplementary information The online version contains supplementary material available at https://doi.org/10.1038/s41467-024-51620-2.

Correspondence and requests for materials should be addressed to Roman Jerala or Mojca Benčina.

Peer review information *Nature Communications* thanks Rajaraman Eri and the other anonymous, reviewers for their contribution to the peer review of this work. A peer review file is available.